Spin relaxation in graphene with self-assembled cobalt porphyrin molecules

Omar, S.; Gurram, M.; Vera-Marun, I. J.; Zhang, X.; Huisman, E. H.; Kaverzin, A.; Feringa, B. L.; van Wees, B. J.

Published in:
Physical Review. B: Condensed Matter and Materials Physics

DOI:
10.1103/PhysRevB.92.115442

Publication date:
2015

Spin relaxation in graphene with self-assembled cobalt porphyrin molecules

S. Omar,[1,*] M. Gurram,[1] I. J. Vera-Marun,[1,2] X. Zhang,[3] E. H. Huisman,[1] A. Kaverzin,[1] B. L. Feringa,[3] and B. J. van Wees[1]

[1]*Physics of Nanodevices, Zernike Institute for Advanced Materials, University of Groningen, Nijenborgh 4, 9747 AG Groningen, Netherlands*

[2]*School of Physics and Astronomy, The University of Manchester, Manchester M13 9PL, United Kingdom*

[3]*Stratingh Institute for Chemistry, Zernike Institute for Advanced Materials, University of Groningen, Nijenborgh 4, 9747 AG Groningen, Netherlands*

(Received 20 April 2015; revised manuscript received 12 July 2015; published 25 September 2015)

In graphene spintronics, interaction of localized magnetic moments with the electron spins paves a new way to explore the underlying spin-relaxation mechanism. A self-assembled layer of organic cobalt porphyrin (CoPP) molecules on graphene provides a desired platform for such studies via the magnetic moments of porphyrin-bound cobalt atoms. In this work a study of spin-transport properties of graphene spin-valve devices functionalized with such CoPP molecules as a function of temperature via nonlocal spin-valve and Hanle spin-precession measurements is reported. For the functionalized (molecular) devices, we observe a decrease in the spin-relaxation time τ_s even up to 50%, which could be an indication of enhanced spin-flip scattering of the electron spins in graphene in the presence of the molecular magnetic moments. The effect of the molecular layer is masked for low-quality samples (low mobility), possibly due to dominance of Elliot-Yafet-type spin relaxation mechanisms.

DOI: 10.1103/PhysRevB.92.115442 PACS number(s): 85.75.−d, 73.22.Pr, 75.76.+j

I. INTRODUCTION

Graphene, a one-atom-thick layer of sp^2 carbon atoms, has potential for spintronic applications due to theoretically predicted high spin-relaxation time ($\tau_s \approx 100$ ns) and long spin-diffusion length ($\lambda_s \approx 100$ μm) [1,2]. These exceptional properties are attributed to negligible spin-orbit coupling and weak hyperfine interaction due to the low atomic mass of carbon [3]. However, the maximum reported experimental values demonstrate λ_s of about 12 μm [4] for encapsulated graphene and τ_s of about 2.7 ns for the hydrogenated graphene [5], which although remarkable when compared with other metals and semiconductors, are still lower than the theoretically predicted values by more than an order of magnitude. A mismatch between theory and experiments suggests external factors such as impurities/defects present near the graphene lattice, which dominate the spin-relaxation process and result in a lower value for λ_s.

In order to probe the role of impurities on spin transport, one can systematically introduce them to graphene. In recent years, different research groups have demonstrated several ways of introducing impurities (magnetic and nonmagnetic) in graphene such as doping with adatoms, introducing defects, and chemical functionalization [6–10], with each method introducing a different spin-relaxation source. For example, heavy-metal atoms such as Au can change the spin-transport properties in graphene via spin-orbit coupling [11]. On the other hand, light-metal (Mg) ions can introduce charge impurity scattering of spins in graphene [12], although the experimental study rules out the role of this mechanism [13]. A significant change in the spin-transport properties of graphene was reported in the presence of magnetic moments [14], which can be introduced via hydrogenation or by introducing vacancies in the graphene lattice. Remarkably, recent weak localization measurements on graphene [15] also show that magnetic impurities could play a key role in limiting the spin-relaxation time in graphene. It has been shown theoretically that [16,17] if the localized moments are present at adatoms, they can act as spin hot spots and enhance the spin-relaxation process via resonant scattering. Therefore, the recent findings serve as an imperative to introduce magnetic impurities in graphene and investigate their effect on the spin transport.

Introducing the impurities via the methods described above may damage the graphene lattice and modify its electronic band structure [18]. Alternatively, the self-assembly of molecular layers on graphene is a nondestructive way to functionalize the graphene surface, and one can still tune the electronic properties of this two-dimensional material [19]. Recently, Zhang reported the self-assembly of porphyrin ligand-bound cobalt atoms (CoPP) on top of a graphene surface [20]. Porphyrins are attached to graphene via weak van der Waals interactions, while the cobalt atoms do not form any chemical bond with graphene in contrast to the direct deposition of metal atoms or ions as discussed above [21]. Therefore, the self-assembly is not supposed to change the electronic properties of graphene significantly. On the other hand, cobalt atoms have an unpaired spin ($S = 1/2$), which can act as a localized magnetic moment.

In this work, we study spin-transport properties of a CoPP-graphene system as a function of temperature, using nonlocal spin valve and Hanle spin-precession measurements. After the self-assembly of magnetic molecules, a reduced τ_s up to 50% with a lowered spin-diffusion coefficient D_s is obtained compared to the values for the sample without functionalization (pristine sample). A pronounced effect of the molecular layer was observed for samples with high mobility and a high diffusion coefficient, alluding to the sample quality playing an important role in determining the spin-transport properties in graphene, in contrast to previous studies [22].

II. DEVICE FABRICATION

Graphene spin-valve devices are prepared using highly oriented pyrolytic graphite (HOPG), which has a very low

*Corresponding author: s.omar@rug.nl

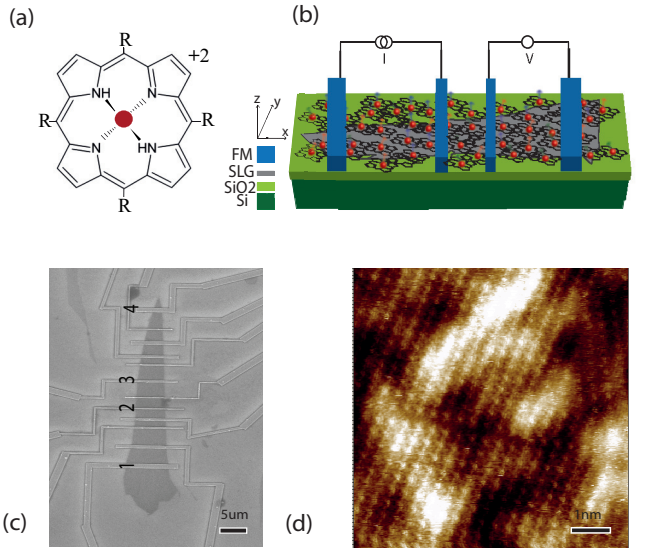

FIG. 1. (Color online) (a) Molecular structure of a cobalt-bound porphyrin (CoPP) complex. Co^{++} (red circle) is the central atom in the complex, surrounded by the porphyrin ligand. In the porphyrin ring R represents a long-chain alkyl group ($C_{10}H_{21}$), which is responsible for making weak van der Waals interaction with graphene during the self-assembly. (b) Nonlocal measurement scheme for a graphene spin valve. Graphene (in gray) with a self-assembly of cobalt porphyrin molecules on top (cobalt magnetic moments in red) is probed with ferromagnetic tunnel contacts (in blue). (c) Scanning electron micrograph (SEM) of sample A. The distance between contacts 2 and 3 (transport channel) is 5 μm. Outer contacts are chosen far enough from the inner ones to make sure that they do not affect the spin transport. (d) A scanning tunneling microscopy (STM) image of CVD graphene functionalized with cobalt porphyrin molecules on top (scan area 39 nm^2) on Si/SiO_2 substrate, which demonstrates an ordered self-assembly of the CoPP molecules on graphene. A bright spot in the image corresponds to the core of the porphyrin molecule.

amount of impurities (ZYA grade, supplier: SPI). Graphene is mechanically exfoliated onto a precleaned Si/SiO_2 substrate (300-nm-thick SiO_2), where n^{++} doped Si is used as a back-gate electrode. Ferromagnetic (FM) contacts are patterned via electron beam lithography on the poly (methyl methacrylate) (PMMA) coated graphene flake. Then 0.4 nm of titanium is deposited in two steps, each step followed by oxidation to define a tunnel barrier, which is to overcome the conductivity mismatch problem [23]. The deposited Ti oxide is only present under the contacts; the rest of the graphene surface is uncovered. On top of the oxide barrier we deposit 35 nm of cobalt for the spin-selective contacts. To prevent oxidation of the ferromagnetic electrodes, the contacts are covered with a 3-nm-thick aluminum layer followed by the lift-off process. A lock-in amplifier detection technique is used to measure the charge- and the spin-transport properties of our samples. All the measurements are carried out using a cryostat in vacuum ($\sim 1 \times 10^{-7}$ mbar) at different temperatures between 4 and 300 K. First, the sample is characterized in its pristine state. Afterwards, the magnetic impurities are added to the sample, and the change in the charge- and spin-transport properties is measured. In order to equip graphene with magnetic molecules, a cobalt porphyrin solution (concentration of 0.56 mg/mL in tetradecane) is drop cast on top of the device and left to dry for 10 min. The residual porphyrin layers on top are removed by rinsing the device with hexane [Fig. 1(b)]. Since the exfoliated samples on the insulating SiO_2 substrate are not big enough to perform scanning tunneling microscopy (STM), in order to confirm the self-assembly of porphyrins on graphene we perform STM on the large-area chemical vapor deposition (CVD) graphene-CoPP system. An STM image [Fig. 1(d)] of a CVD graphene sample (Si/SiO_2 substrate) with the CoPP molecules on top confirms the self-assembly of cobalt porphyrin molecules on graphene.

III. RESULTS AND DISCUSSION

We report the measurements for three samples, prepared under identical conditions. For discussion, they are labeled samples A, B, and C. A scanning electron microscope (SEM) image of sample A is shown in Fig. 1(c).

A. Charge transport

For the charge-transport measurements, an alternating current (ac) is applied between contacts 1 and 4, and the voltage is measured between contacts 2 and 3 [Fig. 1(c)]. In order to measure the carrier density dependence of the graphene resistivity (Dirac curve), we sweep the back-gate voltage. After the self-assembly of the CoPP molecules on the sample, the gate dependence is found to have positive hysteresis at room temperature (inset Fig. 2), which alludes to a charge-transfer process between graphene and the CoPP molecules [24,25]. At

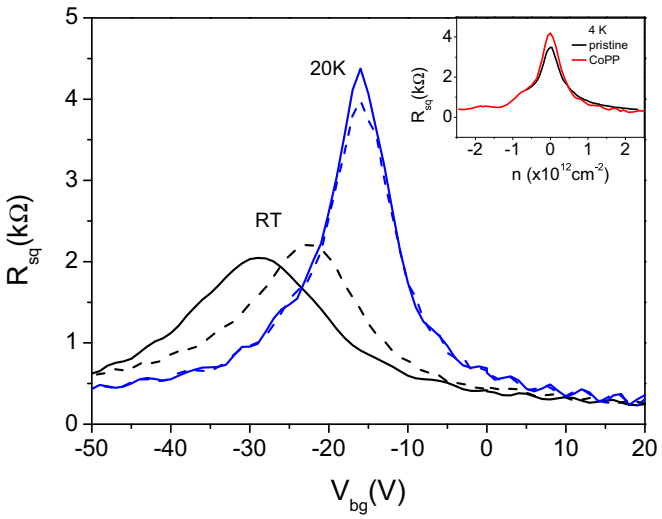

FIG. 2. (Color online) Resistivity as a function of gate voltage for the CoPP device (sample A) at different temperatures. Solid (dashed) lines correspond to the forward (backward) sweeping direction of the back-gate voltage. The CoPP device shows hysteresis at room temperature (black curve), which disappears at low temperatures (blue curve). Hysteresis at RT indicates a charge-transfer process between the CoPP molecules and graphene, which disappears at low temperatures due to freezing of the charged states in the molecules [24]. A comparison between the Dirac measurement for the pristine state and the CoPP state of sample A is shown in the inset (at 4 K). After functionalization, the sheet resistance increases near the charge neutrality point, which is not significant at high carrier densities.

low temperatures charge states are frozen in the molecules, and no hysteresis is observed. The field-effect electron mobility μ_e for the pristine device is 7100 cm^2 V^{-1} s^{-1}, and for the CoPP device $\mu_e \sim 5000$ cm^2 V^{-1} s^{-1}, with both mobilities calculated at room temperature (RT) for a carrier density $\sim 10^{12}$ cm^{-2}. Contact resistances R_c for all the samples were high enough ($\geqslant 1.5\,\mathrm{k}\Omega$) to be in the noninvasive regime, as described in Ref. [23].

B. Spin transport

For the spin-transport measurements, a four-probe nonlocal detection scheme is used [Fig. 1(b)]. This method allows us to decouple the charge and spin current paths and thus minimize the charge contribution to the detected spin signal ($R_{NL} = V_{NL}/I$) [26]. The spin-valve measurement is performed by first setting a high magnetic field $\vec{B}$ along the y direction [Fig. 1(b)], so all the FM electrodes are magnetized along the field (parallel configuration). Then sweeping the field in the opposite direction, the electrodes reverse their magnetization at different fields depending on their coercivity, leading to an antiparallel configuration between the inner injector and the detector electrodes, which appears as a switch in the nonlocal signal. At high magnetic field, all the electrodes are again magnetized in the same direction in the parallel configuration. The difference between the parallel and the antiparallel signals is the spin-valve signal ΔR_{NL}. The outer contacts are chosen far away from the inner electrodes. In this way their influence on the measured spin signal is eliminated, and we see only two distinct switches that correspond to the magnetization reversal of the inner injector and the inner detector.

Spin-valve measurements for sample A before and after the functionalization are shown in Fig. 3 at different temperatures. For both pristine and functionalized states of the sample, the spin-valve signal shows the switches corresponding to the contact magnetization. However, after the functionalization, the signal magnitude is significantly reduced. At low temperature, the signal magnitude is increased for both the pristine and the CoPP devices (Fig. 3).

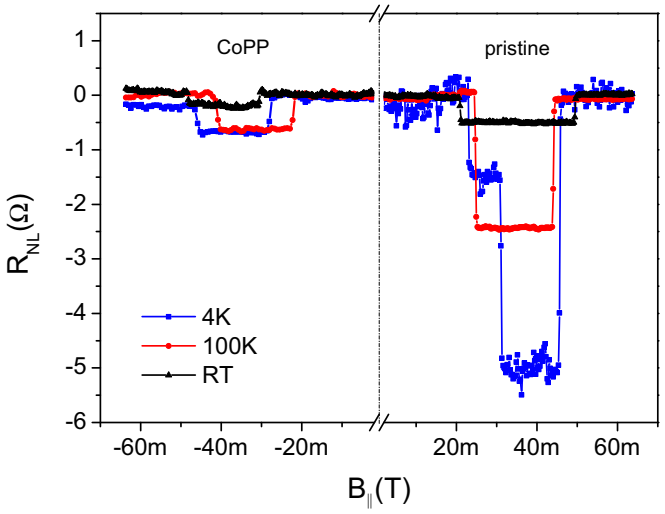

FIG. 3. (Color online) Spin-valve measurements for sample A (all the measurements in the electron-doped regime at $n \sim 10^{12}$ cm^{-2}) are shown in the positive x axis for the pristine state, and those for the device after the functionalization are shown in the negative x axis. A strongly reduced spin-valve signal is observed after the functionalization.

In order to understand the effect of localized magnetic moments on spin transport in graphene, we refer to the exchange-field model, explained by McCreary *et al.* [14]. In this model, an electron spin in graphene can interact with the magnetic moments via an exchange field $\bar{B}_{\mathrm{ex}}$, which is the average exchange field produced by the localized moments. B_{ex} varies spatially and in time in a random fashion and influences locally the Larmor precession of the diffusing spins. The effect of varying precession frequencies at different locations resembles the D'yakonov-Perel mechanism of spin relaxation [27] and is responsible for an additional spin dephasing. In a spin-valve measurement, an enhanced relaxation (a reduced signal) is expected when the moments are randomized. As one starts applying an in-plane magnetic field, the magnetic moments try to align themselves along the field, and their dephasing effect gets suppressed. This feature would appear as a dip in the spin-valve signal. Within this picture, the spin-relaxation rate by the fluctuating exchange field causing the dip is given by the following equation:

$$\frac{1}{\tau_{\mathrm{ex}}} = \frac{\triangle B^2}{\tau_c} \frac{1}{(B_{\mathrm{app},y} + \bar{B}_{\mathrm{ex},y})^2 + \left(\frac{\hbar}{g_e \mu_B \tau_c}\right)^2}, \qquad (1)$$

where $\triangle B$ is the exchange-field fluctuation magnitude, $g_e = 2$ is the gyromagnetic factor of the free electrons, μ_B is the Bohr magneton, $\hbar$ is the reduced Plank constant, and τ_c is the fluctuation correlation time [14]. According to the formula above, the maximum relaxation (dip) in the spin-valve measurement should appear when $B_{\mathrm{app}} = -\bar{B}_{\mathrm{ex}}$. Therefore, the magnetic ordering of the localized moments affects the observation of the dip. For paramagnetic ordering one would observe the dip around $B_{\mathrm{app}} = 0$. On the other hand, for ferromagnetic ordering, there is a nonzero exchange field B_{ex} present ($\bar{B}_{\mathrm{ex}} \neq 0$) even when no external field is applied ($B_{\mathrm{app}} = 0$). Now the dip would occur at finite external applied field and would exhibit hysteresis.

For the measured spin-valve signal for the CoPP device, we do not observe any dip, either around zero or nonzero applied field. The only clear effect of introducing the CoPP molecules is the reduced magnitude of the spin-valve signal. The observed behavior can be explained by considering the magnetic moments playing the role of spin-flip scatterers in the transport channel, which enhance the spin-relaxation process but do not produce a measurable effective exchange field. In order to confirm if the source of the reduced spin signal is due to an enhanced spin-relaxation rate, we now need to measure the spin-transport parameters via Hanle spin-precession measurements.

Hanle precession measurement is a reliable tool to study the spin-transport properties. Here, a magnetic field is applied perpendicular to the direction of the injected spins, which precess around this field $\vec{B}$ with Larmor frequency $\vec{\omega_L} = g_e \mu_B \vec{B}/\hbar$. While sweeping the magnetic field, due to the precession, spins can be reoriented to a direction opposite the injected one, leading to a sign reversal in the spin signal. Simultaneously, they also dephase and result in a lower spin accumulation at higher fields. The Hanle precession can be

fitted with the equation [26]

$$\triangle R_{NL} \propto \int_0^\infty \frac{1}{\sqrt{(4\pi D_s t)}} e^{\frac{-L^2}{4D_s t}} cos(\omega_L t) e^{\frac{-t}{\tau_s}} dt, \qquad (2)$$

where D_s is the spin diffusion coefficient, τ_s the spin relaxation time, L is the distance between the inner injector and the detector electrodes and ω_L is the Larmor frequency.

Referring back to the exchange-field model, a Hanle measurement in the presence of an exchange magnetic field B_{ex} by the magnetic moments would represent a spin precession due to a net field $B_{app} + B_{ex}$. The precession can result in a narrower Hanle shape due to an enhanced g factor [5,14,28] for a paramagnetic ordering of the localized moments. However, for the case of ferromagnetic ordering, we would expect a shifted Hanle peak.

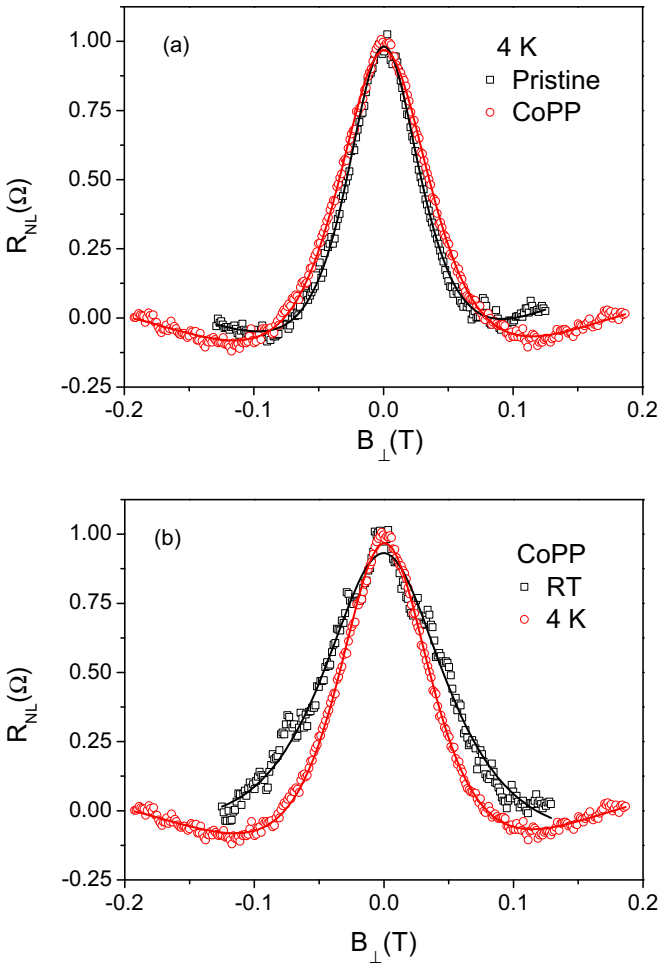

FIG. 4. (Color online) (a) Hanle measurements $[(R_P - R_{AP})/2]$ for the pristine state (black squares) and the CoPP state (red circles) at 4 K (sample B). The corresponding fittings are plotted in line. The curves are normalized with respect to the signal at $B = 0$. After the functionalization Hanle line shape is broadened, indicating a reduced spin-relaxation time τ_s. (b) Hanle measurements for sample B after self-assembly at RT and 4 K. The curves are normalized. Broadening of the black curve (with squares; RT) is dominated by the enhanced D_s. The spin-relaxation time τ_s only changes from 100 ps (RT) to 112 ps (4K). All the measurements were done at fixed carrier density ($n \sim 10^{12}$ cm^{-2}).

Hanle precession curves for both pristine and CoPP devices are shown in Fig. 4. Here, we show the purely spin dependent signal, obtained by subtracting the antiparallel signal from the parallel signal, and the result is fitted via Eq. (2). The plots have been normalized to the value at $B_{app} = 0$ because they clearly demonstrate the change in the Hanle line shape. We observe two general trends for all measured samples. First, the Hanle curve becomes broader after the CoPP self-assembly. This is in contrast to the expected narrowing of the Hanle curve in the presence of a paramagnetic exchange field according to the model described above. The observed broadening indicates a reduction of the spin-relaxation time, in accordance with our interpretation of the signal reduction in spin-valve measurements. Second, upon decreasing the temperature from RT down to 4 K we do not observe any significant narrowing of the Hanle line shape which could be interpreted as an enhanced g factor. On the contrary, the typical linewidths and extracted spin lifetimes are not strongly dependent on temperature.

A summary of the extracted spin parameters for all samples studied in this work is presented in Fig. 5. For sample A we observed the strongest effect of the molecular layer on the spin parameters. In its pristine state, the extracted spin-relaxation time τ_s is in the range of 300–400 ps for all the measured temperatures, with a corresponding spin-diffusion length λ_s ($=\sqrt{D_s \tau_s}$) of 3–4.5 μm. On the other hand, after self-assembly sample A exhibited a strongly reduced τ_s in the range 100–200 ps and a correspondingly lower $\lambda_s \sim$ 2–2.5 μm. Interestingly, we did not observe any significant temperature dependence for the extracted τ_s in the measured temperature range, which would have otherwise been expected due to the presence of an effective exchange field via localized molecular paramagnetic moments [14,28]. Therefore, the added magnetic molecules seem to only increase the spin-relaxation rate via the introduction of more spin-flip scattering events.

Furthermore, we also observed a minor reduction of the extracted spin-diffusion coefficient D_s after self-assembly, consistent with the observed reduction in mobility as discussed in Fig. 2. Note that the reliability of a Hanle fit is typically established by comparing the agreement between the extracted spin-diffusion coefficient D_s and the charge-diffusion coefficient D_c [5,14,23]. The latter can be independently calculated via the resistivity of the sample at a known density of states ν using the Einstein relation $D_c = 1/R_{sq} e^2 \nu$. In the absence of electron-electron interaction D_c and D_s should match [30]. As shown in Table I, both parameters are in reasonable agreement, confirming the validity of the Hanle analysis.

It is worth mentioning that the earlier work of molecular doping on graphene [22] did not exhibit any measurable change in the spin-transport properties of graphene, while the charge-transport properties were modified. However, we find that sample quality, as determined by the magnitude of the diffusion coefficient (D_c, D_s) or electronic mobility μ_e, plays an important role in the influence that the cobalt porphyrin molecular layer exerts on the spin-transport parameters. For example, for sample B we do not observe a significant change in D_s and τ_s after self-assembly. This reduced sensitivity can be attributed to its low mobility (and diffusion coefficient), which in the pristine state was $\sim$2000 cm^2 V^{-1} s^{-1}, almost a factor of 3.5 times lower than that for sample A. On the other hand, for sample C, which had a comparatively better quality ($D_s \sim$

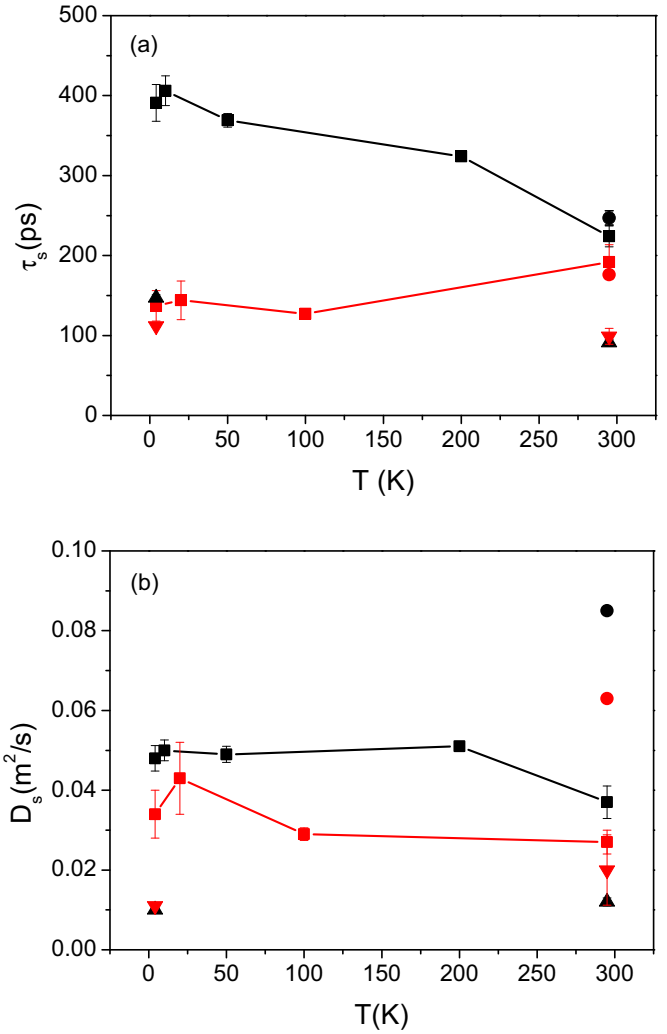

FIG. 5. (Color online) A summary of (a) τ_s and (b) D_s, extracted from Hanle analysis, for samples A (squares plus line), B (triangle), and C (circle) before (black) and after (red) the functionalization. Black data correspond to the pristine state, and red data are for the CoPP state of the samples. Reduced τ_s and D_s were observed for the samples after the functionalization with a weak temperature dependence, which rules out any exchange coupling between the localized magnetic moments and the electron spins in graphene [28] and indicates an enhanced spin-flip process, where the present magnetic moments play only the role of spin-flip scatterers. The effect of the molecular layer is determined by the sample quality (μ_e, D) in the pristine state. Since samples A and C have higher mobility and diffusion coefficient, τ_s is highly reduced for these samples after the functionalization. Sample B, having lower mobility, did not show any significant change in τ_s.

0.1 m^2/s), we again observed a significant reduction of 30% on the spin-relaxation time, confirming our initial observations.

A significant reduction in τ_s, with a simultaneous moderate reduction in D_s, is inconsistent with the picture of localized magnetic moments creating an effective exchange field as discussed above [14,28] or a model where localized states act as spin reservoirs [31]. Both models imply a significant increase of the extracted τ_s and a proportionally reduced D_s, which can be understood via an enhanced g factor and the symmetry of the Hanle equation [5,28]. Even for a reduced g factor, one would observe a reduced τ_s and an enhanced D_s, which also does not comply with our observation. Furthermore, both models are also expected to show a strong temperature dependence, which is not observed here.

TABLE I. A summary of D_c and D_s (in m^2/s) for samples A, B, and C before (pristine) and after (CoPP) functionalization. For all the samples, D_c and D_s are approximately in the same order. For sample A, D_c in the pristine state is found around 0.05 m^2/s. We also sometimes observed an asymmetry in the Dirac curve at different temperatures. This asymmetry arises due to contact-induced doping in different regions [29], resulting in a different value for D_c at different temperatures.

	4 K				RT			
	Pristine		CoPP		Pristine		CoPP	
	D_c	D_s	D_c	D_s	D_c	D_s	D_c	D_s
A	0.052	0.048	0.039	0.034	0.100	0.037	0.050	0.027
B	0.010	0.010	0.011	0.010	0.014	0.012	0.020	0.020
C				0.12		0.085		0.063

The reduction in the spin-transport parameters indicates that the main role of the Co-porphyrin molecular layer is to act as an extra source of spin-flip scattering. This interpretation is consistent with the lack of sensitivity to the molecular layer by low-quality samples, where the initial spin-relaxation rate was already large and therefore masks the relaxation process introduced by the molecular layer. In addition, the concomitant reduction in D_s and τ_s observed can be partially understood by the enhanced momentum scattering introduced by the molecular layer since in single-layer graphene the leading spin-relaxation mechanism is of the Elliot-Yafet type, which results in the proportionality relation $\tau_s \propto D$ [32–34]. This observation is interesting since previous experiments ruled out the role of the mobility dependence of τ_s [22] or seemed to observe an opposite relation between τ_s and μ_e, i.e., higher spin lifetime for lower-mobility samples [29].

IV. CONCLUSIONS

To summarize, we observed a change in both the charge- and spin-transport properties of graphene in the presence of cobalt porphyrin molecules. In the charge-transport measurements, we observe an increase in the graphene-sheet resistance after functionalization due to cobalt porphyrin molecules interaction with graphene via weak van der Waals forces. For the spin-transport measurements we observe lower values of τ_s and λ_s for the CoPP-graphene system compared to the pristine one. The measurements are not strongly temperature dependent, which is not consistent with the presence of an exchange field and suggests that the exchange interactions, if present, are random. At present, however, we cannot explicitly identify the origin, either due to exchange interaction or due to spin-orbit interaction, of the enhanced spin relaxation produced by the magnetic impurities. The changes are also sensitive to the sample quality (D, μ_e) in the pristine state and are masked for a lower value of the mobility or diffusion coefficient, indicating also the presence of an Elliot-Yafet-type spin-relaxation mechanism.

ACKNOWLEDGMENTS

We acknowledge J. G. Holstein, H. M. de Roosz, and H. Adema for their technical assistance. We would like to thank M. H. D. Guimãraes and J. J. van den Berg for their help in sample preparation. This research work was financed under the EU graphene flagship program (Grant no. 637088) and supported by the Zernike Institute for Advanced Materials, the Ministry of Education Culture and Science (Gravitation program 024.601035, B.L.F.), and the Nederlandse Organisatie voor Wetenschappelijk (NWO).

[1] V. K. Dugaev, E. Y. Sherman, and J. Barnaś, Phys. Rev. B **83**, 085306 (2011).
[2] H. Min, J. E. Hill, N. A. Sinitsyn, B. R. Sahu, L. Kleinman, and A. H. MacDonald, Phys. Rev. B **74**, 165310 (2006).
[3] M. Wojtaszek, I. J. Vera-Marun, E. Whiteway, M. Hilke, and B. J. van Wees, Phys. Rev. B **89**, 035417 (2014).
[4] M. H. D. Guimarães, P. J. Zomer, J. Ingla-Aynés, J. C. Brant, N. Tombros, and B. J. van Wees, Phys. Rev. Lett. **113**, 086602 (2014).
[5] M. Wojtaszek, I. J. Vera-Marun, T. Maassen, and B. J. van Wees, Phys. Rev. B **87**, 081402 (2013).
[6] R. R. Nair, M. Sepioni, I.-L. Tsai, O. Lehtinen, J. Keinonen, A. V. Krasheninnikov, T. Thomson, A. K. Geim, and I. V. Grigorieva, Nat. Phys. **8**, 199 (2012).
[7] L. Xie, X. Wang, J. Lu, Z. Ni, Z. Luo, H. Mao, R. Wang, Y. Wang, H. Huang, D. Qi, R. Liu, T. Yu, Z. Shen, T. Wu, H. Peng, B. Özyilmaz, K. Loh, A. T. S. Wee, Ariando, and W. Chen, Appl. Phys. Lett. **98**, 193113 (2011).
[8] P. Esquinazi, D. Spemann, R. Höhne, A. Setzer, K.-H. Han, and T. Butz, Phys. Rev. Lett. **91**, 227201 (2003).
[9] J. Červenka, M. I. Katsnelson, and C. F. J. Flipse, Nat. Phys. **5**, 840 (2009).
[10] X. Hong, S.-H. Cheng, C. Herding, and J. Zhu, Phys. Rev. B **83**, 085410 (2011).
[11] K. Pi, W. Han, K. M. McCreary, A. G. Swartz, Y. Li, and R. K. Kawakami, Phys. Rev. Lett. **104**, 187201 (2010).
[12] C. Ertler, S. Konschuh, M. Gmitra, and J. Fabian, Phys. Rev. B **80**, 041405 (2009).
[13] A. G. Swartz, J.-R. Chen, K. M. McCreary, P. M. Odenthal, W. Han, and R. K. Kawakami, Phys. Rev. B **87**, 075455 (2013).
[14] K. M. McCreary, A. G. Swartz, W. Han, J. Fabian, and R. K. Kawakami, Phys. Rev. Lett. **109**, 186604 (2012).
[15] M. B. Lundeberg, R. Yang, J. Renard, and J. A. Folk, Phys. Rev. Lett. **110**, 156601 (2013).
[16] D. Kochan, M. Gmitra, and J. Fabian, Phys. Rev. Lett. **112**, 116602 (2014).
[17] D. Soriano, D. V. Tuan, S. M.-M. Dubois, M. Gmitra, A. W. Cummings, D. Kochan, F. Ortmann, J.-C. Charlier, J. Fabian, and S. Roche, 2D Mater. **2**, 022002 (2015).
[18] D. W. Boukhvalov and M. I. Katsnelson, Appl. Phys. Lett. **95**, 023109 (2009).
[19] X. Zhang, E. H. Huisman, M. Gurram, W. R. Browne, B. J. van Wees, and B. L. Feringa, Small **10**, 1735 (2014).
[20] X. Zhang, Ph.D. thesis, University of Groningen, 2013.
[21] C. F. Hermanns, K. Tarafder, M. Bernien, A. Krüger, Y.-M. Chang, P. M. Oppeneer, and W. Kuch, Adv. Mater. **25**, 3473 (2013).
[22] W. Han, J.-R. Chen, D. Wang, K. M. McCreary, H. Wen, A. G. Swartz, J. Shi, and R. K. Kawakami, Nano Lett. **12**, 3443 (2012).
[23] T. Maassen, I. J. Vera-Marun, M. H. D. Guimãraes, and B. J. van Wees, Phys. Rev. B **86**, 235408 (2012).
[24] D. Wang, X. Liu, L. He, Y. Yin, D. Wu, and J. Shi, Nano Lett. **10**, 4989 (2010).
[25] A. Veligura, P. J. Zomer, I. J. Vera-Marun, C. Jzsa, P. I. Gordiichuk, and B. J. v. Wees, J. Appl. Phys. **110**, 113708 (2011).
[26] N. Tombros, C. Jozsa, M. Popinciuc, H. T. Jonkman, and B. J. van Wees, Nature (London) **448**, 571 (2007).
[27] J. Fabian, A. Matos-Abiague, C. Ertler, P. Stano, and I. Zutic, Acta Phys. Slov. **57**, 565 (2007).
[28] B. Birkner, D. Pachniowski, A. Sandner, M. Ostler, T. Seyller, J. Fabian, M. Ciorga, D. Weiss, and J. Eroms, Phys. Rev. B **87**, 081405 (2013).
[29] F. Volmer, M. Drögeler, E. Maynicke, N. von den Driesch, M. L. Boschen, G. Güntherodt, C. Stampfer, and B. Beschoten, Phys. Rev. B **90**, 165403 (2014).
[30] C. P. Weber, N. Gedik, J. E. Moore, J. Orenstein, J. Stephens, and D. D. Awschalom, Nature (London) **437**, 1330 (2005).
[31] T. Maassen, J. J. van den Berg, E. H. Huisman, H. Dijkstra, F. Fromm, T. Seyller, and B. J. van Wees, Phys. Rev. Lett. **110**, 067209 (2013).
[32] C. Józsa, T. Maassen, M. Popinciuc, P. J. Zomer, A. Veligura, H. T. Jonkman, and B. J. van Wees, Phys. Rev. B **80**, 241403 (2009).
[33] W. Han and R. K. Kawakami, Phys. Rev. Lett. **107**, 047207 (2011).
[34] T.-Y. Yang, J. Balakrishnan, F. Volmer, A. Avsar, M. Jaiswal, J. Samm, S. R. Ali, A. Pachoud, M. Zeng, M. Popinciuc, G. Güntherodt, B. Beschoten, and B. Özyilmaz, Phys. Rev. Lett. **107**, 047206 (2011).